Passive Wireless Strain Sensors Using Microfabricated Magnetoelastic Beam Elements

Venkatram Pepakayala, Scott R. Green, and Yogesh B. Gianchandani

***Abstract*— This paper describes resonant wireless strain sensors fabricated from magnetoelastic alloys. The transduction mechanism is the ΔE effect—the change in stiffness of magnetoelastic materials with applied strain or magnetic field. This is measured as a shift in the resonant frequency and is detected wirelessly using pick-up coils utilizing the magnetoelastic coupling of these materials. The sensors are fabricated from a 28-μm-thick foil of Metglas 2826 MB ($Fe_{40}Ni_{38}Mo_4B_{18}$), a ferromagnetic magnetoelastic alloy, using microelectrodischarge machining. Two sensor types are described—single and differential. The single sensor has an active area of 7 × 2 mm^2, excluding the anchors. At 23°C, it operates at a resonant frequency of 230.8 kHz and has a sensitivity of 13 × 10^3 ppm/mstrain; the dynamic range is 0.05–1.05 mstrain. The differential sensor includes a strain independent reference resonator of area 2 × 0.5 mm^2 in addition to a sensing element of area 2.5 × 0.5 mm^2 that is divided into two segments. The sensor resonance is at 266.4 kHz and reference resonance is at 492.75 kHz. The differential sensor provides a dynamic range for 0–1.85 mstrain with a sensitivity of 12.5 × 10^3 ppm/mstrain at 23°C. The reference resonator of the differential sensor is used to compensate for the temperature dependence of the Young's modulus of Metglas 2826 MB, which is experimentally estimated to be −524 ppm/°C. For an increment of 35°C, uncompensated sensors exhibit a resonant frequency shift of up to 42% of the dynamic range for the single sensor and 30% of the dynamic range of the differential sensor, underscoring the necessity of temperature compensation. The geometry of both types of sensors can be modified to accommodate a variety of sensitivity and dynamic range requirements. [2013-0330]**

***Index Terms*— Strain measurement, magnetoelasticity, resonant sensing, Metglas, ΔE effect.**

I. Introduction

STRAIN GAGES have long been used for applications ranging from structural health monitoring to material testing and evaluation across a wide range of sectors from civil, aerospace, and infrastructure, to medical prostheses. Most strain gages are made from metal foils that must be wired to interface electronics and a power source. Wireless strain sensors that can be remotely accessed are attractive for some applications. An example is the *in vivo* monitoring of implants, where wireless signaling is possibly the only practical way to obtain a long-term strain measurement [1].

Wireless strain sensors can be either powered or passive. Powered sensors require a battery or an energy harvesting system or a combination of the two [2]. Passive sensors do not require an inbuilt power source. The most widely investigated techniques for passive strain sensing utilize inductive coupling, RF electromagnetic backscattering, and surface acoustic waves [3]–[8]. An optical method has also been reported [9]. Passive sensors are usually simpler and more robust than powered kinds. This work presents an RF wireless, passive sensor that utilizes the resonance of magnetoelastic structures.

Magnetoelastic materials have proven to be very versatile for a range of wireless sensing applications and magnetoelastic devices have been used for sensing mass loading [10], viscosity [11], fluid flow [12], pressure [13], position [14], and other physical parameters. The most common transduction methods involve change in resonant frequencies of magnetoelastic elements caused by changes in mass loading, viscosity or magnetic field conditions [10]–[12], [16], [17]. A magnetic field applied to a magnetoelastic material produces a strain in an effect termed Joule magnetostriction. An inverse effect, called the Villari effect, results in the magnetization of material by applied strain. At the heart of both effects lies the rotation of magnetic moments within domains that leads to the magnetization of the material. Joule magnetostriction is moment rotation under an applied magnetic field, whereas Villari effect is the moment rotation under strain. When an alternating magnetic field is applied to a magnetoelastic material, the induced mechanical vibration, through the Joule effect, results in a strain-induced material magnetization, that is the Villari effect. The resonance can be detected by an appropriately positioned coil. A review of magnetoelastic resonant sensors for a wide variety of applications is presented in [18].

Some physical phenomena can be exploited to induce a change in the magnetization state of a material, effectively modifying its permeability. The permeability change can be measured as a change in inductance of a coil or the mutual inductance between two coils wrapped around the magnetoelastic material [12], [13], [19].

Both the aforementioned techniques – change in resonant frequency or change in magnetization – can be used for strain sensing purposes. Strain applied to a magnetoelastic material results in magnetization and change in permeability through the Villari effect, which can then be detected using a read-out coil [20]–[25]. A potential drawback of this technique is that the signal is susceptible to the geometry of the coil and its position relative to the magnetoelastic material.

Manuscript received October 25, 2013; revised February 25, 2014; accepted March 18, 2014. This WIMS2 Project was supported in part by the Food and Drug Administration, Department of Health and Human Services, under Grant 2P50FD00378703. Subject Editor A. Seshia.

The authors are with the Center for Wireless Integrated MicroSensing and Systems, Department of Electrical Engineering and Computer Science, University of Michigan, Ann Arbor, MI 48109 USA (e-mail: venkatp@umich.edu; greensr@umich.edu; yogesh@umich.edu).

Color versions of one or more of the figures in this paper are available online at http://ieeexplore.ieee.org.

Digital Object Identifier 10.1109/JMEMS.2014.2313809

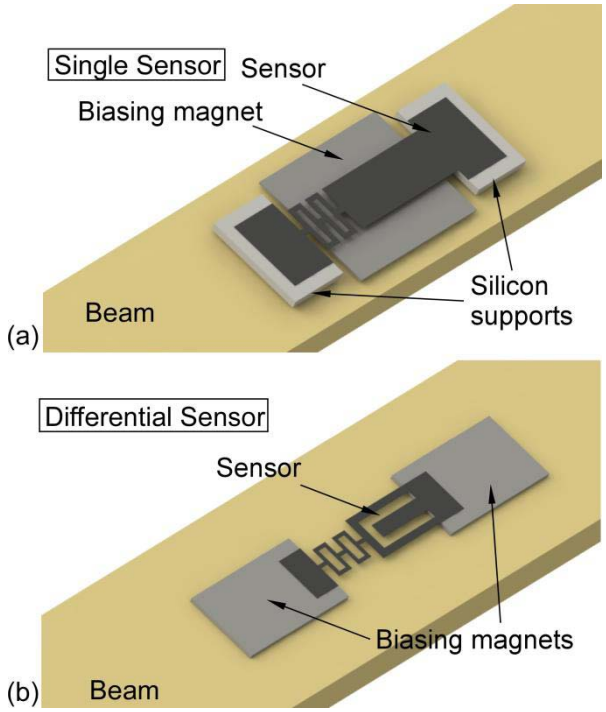

Fig. 1. (a) Assembly of the single sensor showing the silicon supports and bias magnet. (b) Differential sensor suspended on bias magnets with strain-independent cantilevered reference resonator. The sensors are fixed on a test beam.

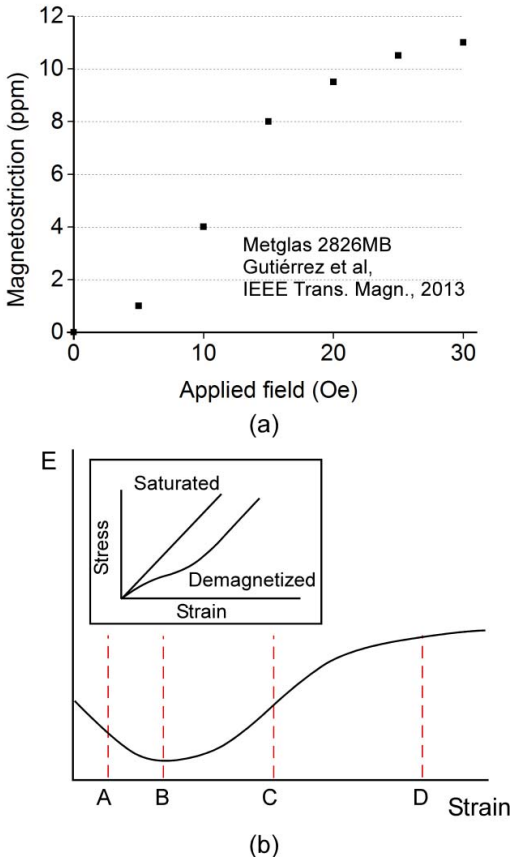

Fig. 2. (a) Magnetostriction as a function of applied field for as-cast Metglas 2826MB, an amorphous magnetostrictive alloy. Due to the presence of demagnetizing fields, the magnetostriction characteristic is highly dependent on material geometry. (b) Small-signal stiffness (slope of the stress-strain curve, shown in the inset) for a typical demagnetized specimen of a magnetoelastic material. Points A, B, C, and D are operating points under increasing magnitude of applied magnetic field.

Another phenomenon observed in magnetoelastic materials – magnetization-induced change in Young's modulus, i.e., the ΔE effect – can be exploited to provide a strain dependence to the resonant frequency. In [26], two magnetoelastic strips held in close proximity were utilized together – one to provide a strain-dependent biasing field for the other, which served as the resonator. The dynamic range was limited by saturation magnetization of the biasing strip and was reported to be ± 50 μstrain.

This paper presents a passive, resonant, strain sensing approach based on the ΔE effect of magnetoelastic materials, where the strain is transferred to a doubly-anchored suspended resonating structure.[1] The resonant response of the structure is detected wirelessly through interrogation coils and is observed as a peak in the frequency spectrum of the coil voltage. A strain-attenuating spring structure is provided to increase the sensor dynamic range by preventing magnetic saturation at low levels of applied strain. Two sensor types are described – single and differential (Fig. 1). Both sensors include doubly-anchored resonant strips; the differential sensor has an additional cantilever exhibiting a strain-independent resonant response. The theory and modeling of the devices are outlined, followed by the design and fabrication. Finally, the experimental methods and results are described.

II. Theory and Modeling

A. General Considerations

The interrogation of resonant magnetoelastic sensors generally involves a small amplitude vibration induced by a sinusoidal stimulation around a bias field. Although magnetostriction is a non-linear phenomenon, the small signal response can be linearized at the bias as expressed by the following pair of equations for a one-dimensional system considering stress and field intensity as the independent variables [28]:

$$\varepsilon = \left.\frac{\partial \varepsilon}{\partial \sigma}\right|_H \sigma + \left.\frac{\partial \varepsilon}{\partial H}\right|_\sigma H \quad (1)$$

$$B = \left.\frac{\partial B}{\partial \sigma}\right|_H \sigma + \left.\frac{\partial B}{\partial H}\right|_\sigma H \quad (2)$$

where σ is stress, ε is strain, B is magnetic flux density and H is magnetic field intensity (all small signal). The partial derivatives are as follows:
$\left.\frac{\partial \varepsilon}{\partial \sigma}\right|_H$ is the compliance at constant H, s^H;
$\left.\frac{\partial B}{\partial H}\right|_\sigma$ is the permeability at constant stress, μ^σ;
and $\left.\frac{\partial \varepsilon}{\partial H}\right|_\sigma$ and $\left.\frac{\partial B}{\partial \sigma}\right|_H$ are both represented by d, the magnetostrictive coefficient.

The magnetostrictive coefficient (also called small-signal magnetostrictivity), d, is the slope of the magnetostriction curve as a function of an applied DC magnetic field. The magnetostriction curve for Metglas 2826MB, an amorphous magnetoelastic material, is shown in Fig. 2(a) [29]. A bias field that is too high or too low results in a low value of d

[1]Portions of this paper have appeared in conference abstract form in [27].

and lower response from the sensor. This bias field is usually provided using a permanent magnet placed in proximity to the magnetostrictive material.

For this work, equations (1) and (2) were used to implement a coupled magnetomechanical simulation model in COMSOL Multiphysics 4.3 following the approach described in [10]. This model was used to obtain the resonant frequencies and mode shapes of the sensor designs.

B. The ΔE Effect

In a magnetoelastic material under stress, strain is produced by two processes: the first is elastic strain (as produced in all materials); the second is from the Villari effect which represents magnetic moment rotation. In materials with strong spin-orbit coupling, rotation of magnetic moment results in rotation of electron clouds. If the electron charge cloud is anisotropically shaped, its rotation effectively results in strain [30]. The Young's modulus at a fixed DC magnetic bias field, B_0 can then be written as:

$$E|_{B_0} = \frac{\sigma}{\varepsilon_{el} + \varepsilon_{mag}} \tag{3}$$

where ε_{el} is the elastic strain and ε_{mag} is the strain due to material magnetization.

The ε_{mag} component of strain reduces as the material is exposed to higher stress levels and consequently, the Young's modulus increases. Additionally, if the magnetic field or applied stress is such that the material is magnetically saturated, the only incremental contribution to strain is elastic, and the ΔE effect saturates. Fig. 2(b) shows a typical stress-strain relationship and the slope of the stress-strain curve, i.e. Young's modulus, as a function of stress [31]. Points A, B, C and D indicate different bias levels of the magnetic field, that result in different responses. Tuning the biasing magnetic field or mechanically pre-stressing the sensor during attachment shifts the baseline operating point of the sensor. This property can be employed to allow measurement of both tensile and compressive strains.

C. Material Considerations

A range of magnetoelastic materials – both crystalline and amorphous – have been used in transducer applications [32]–[35]. Crystalline rare-earth magnetoelastic alloys like Terfenol-D, while showing excellent magnetostriction, have low tensile strength and are brittle [36]. These materials can also require a high bias field for resonant devices. For instance, Terfenol-D can require bias fields of the order of hundreds of oersteds while Metglas 2826MB, an amorphous alloy, requires a bias field of a few oersteds [37], [38]. The lower bias field allows the use of smaller magnets and reduces the overall sensor size. Amorphous materials can also be tailored to have a high magnetomechanical coupling coefficient (i.e. higher efficiency for conversion of magnetic energy to mechanical energy and vice-versa) through the process of annealing in a magnetic field – a feature which can be advantageous in transducer applications [39]–[41]. The ΔE effect in amorphous magnetoelastic materials can also be modified by annealing under varying temperature and magnetic field conditions [42]. The availability of amorphous magnetoelastic metallic glasses in the form of thin sheets that can be machined to small form factors has contributed to their development for a range of resonant sensing applications. All these considerations favor the use of amorphous materials for resonant strain sensing.

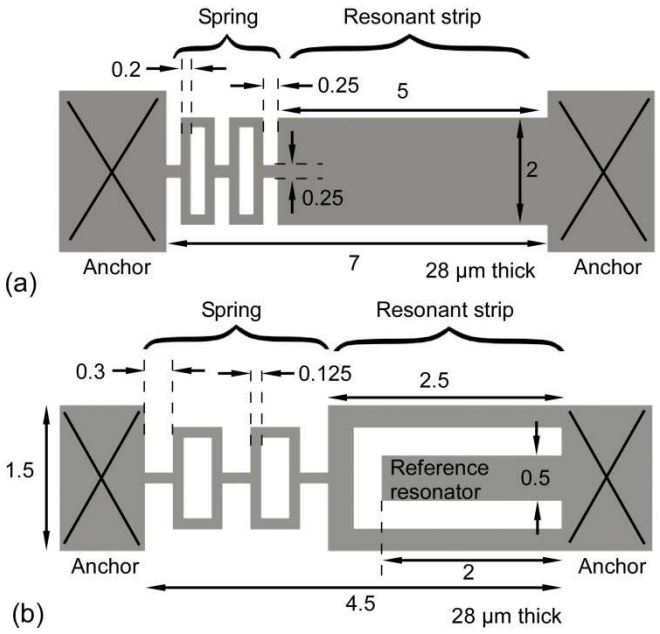

Fig. 3. Sensor designs: (a) Single sensor; (b) differential sensor. All dimensions in mm.

In this work the sensors are made from Metglas 2826MB ($Fe_{40}Ni_{38}Mo_4B_{18}$), an amorphous magnetoelastic alloy manufactured by Metglas, Inc, Conway, SC. Available in foils measuring 28 μm thick, it can be micromachined using micro-electrodischarge machining (μEDM) or photochemical machining (PCM). It has a saturation magnetostriction of 12 ppm and a DC permeability greater than 50000 [43]. The high permeability can serve to attract and direct the magnetic biasing field along the sensor, so the bias field need not be perfectly aligned with the sensor.

The biasing magnetic field required for resonant operation of the sensor is provided by a permanent magnet made using 50 μm thick sheets of Arnokrome 5 (Arnold Magnetic Technologies Corp., Rochester, NY) – an iron-manganese alloy [44]. It shows a remanence of 12–16 kG and a coercivity of 20–50 Oe.

III. Design and Fabrication

A. Resonating Elements

Two types of strain sensors are investigated in this effort – single and differential (Fig. 3). The sensing element for both types consists of a doubly-anchored suspended strip of Metglas 2826MB. It can be divided into two parts – a resonant strip and a spring. The spring serves to attenuate the strain in the resonant strip. This is necessary for sensor to provide a wide dynamic range, as the ΔE effect of magnetoelastic materials typically saturates at low levels of strains [26].

Higher strains do not result in any appreciable change in stiffness and consequently no change in resonant frequency. While the geometry and boundary conditions of the sensors are such that both transverse (i.e. bending) and longitudinal modes exist, the first longitudinal mode of each sensor type is typically dominant in the wireless response of the sensor because it provides the largest unidirectional strain (i.e. mainly compressive or tensile at a given instant in time), which results in the strongest response magnetic field.

In the single strain sensor, the resonating element is 5×2 mm^2 in area. This area determines the strength of the transmitted RF signal. The spring is 2×2 mm^2 in area, and is made with 200 μm wide elements. The entire structure is 28 μm thick. In the differential sensor, the sensing element is divided into two parallel sections. The sensing element in each section is 2.5×0.25 mm^2 whereas the shared spring element is 2×1 mm^2. The differential sensor also contains a reference resonator. This is a cantilever and is unaffected by any strain applied to the sensor. All elements are 28 μm thick. The reference resonator is helpful because the Young's modulus of the sensor material varies with temperature [45], [46]. This (common mode) variation in the absence of strain can be compensated by the response of the reference element. For small shifts in resonant frequency, Δf, to which a linear approximation can be applied:

$$\left.\frac{\Delta f}{f_0}\right|_{B_0}(\varepsilon, T) \approx S_T(\varepsilon)\,\Delta\varepsilon + S_\varepsilon(T)\Delta T \tag{4}$$

where B_0 is the biasing magnetic flux density through the resonating element, assumed to be invariant; f_0 is the baseline resonant frequency; $S_T(\varepsilon)$ is $\frac{\partial}{\partial\varepsilon}\left(\frac{\Delta f}{f_0}\right)_T$, the sensitivity to strain at constant temperature; and $S_\varepsilon(T)$ is $\frac{\partial}{\partial T}\left(\frac{\Delta f}{f_0}\right)_\varepsilon$, the sensitivity to temperature at constant strain. The term $S_\varepsilon(T)$ at zero strain is obtained from the response of the cantilever reference resonator in the differential device, whereas the sensing element of the differential sensor and the single sensor each provide the total sum. The $\Delta\varepsilon$, therefore, must be calculated from the sum. Of course, $\Delta\varepsilon$ itself has a temperature dependence based on the expansion mismatch between the sensor and the substrate to which it is attached. However, the calculated strain does not differentiate between thermal and mechanical sources of strain.

Initial experiments indicated that the ΔE effect of Metglas 2826MB saturates at about 50 μstrain. In this work, the springs were designed to limit the strain in the resonant strip to this value at the target strain of 2 mstrain on the entire sensor. Further, the sensors were sized to ensure that their resonant frequencies were within the excitation and detection range of the test setup. The compromise between sensor size and signal strength were also considered in selecting the final dimensions which are described in Fig. 3.

The coupled magnetomechanical model previously described was used to simulate the resonant frequencies and mode shapes for the devices. For the single sensor the simulated resonant frequency was 230 kHz. For the differential sensor, the resonant frequency of the sensing element was 276 kHz, whereas the resonant frequency for the reference was 496 kHz. The simulated mode shapes for both the single and differential sensors are shown in Fig. 4.

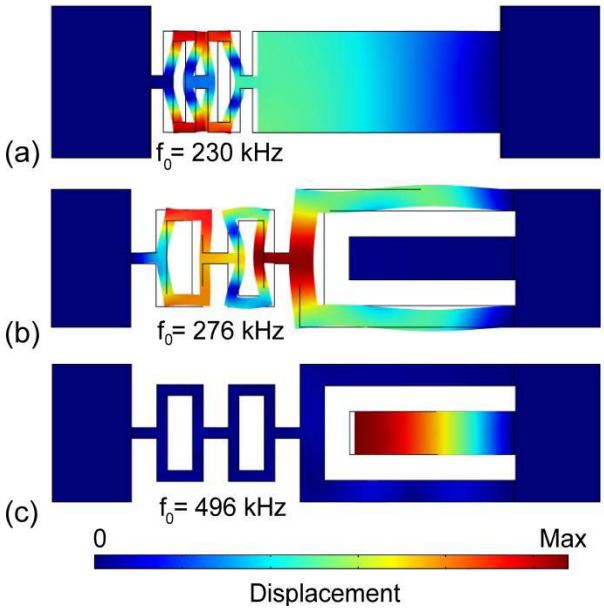

Fig. 4. Simulated mode shapes for single and differential sensor. (a) Single sensor, (b) differential sensor, sensing element, and (c) differential sensor, reference element. The Young's modulus was assumed to be 120 GPa in this simulation.

The sensor shows a shift in resonant frequency shift not only due to ΔE effect but also because of a change in its equation of motion in presence of axial loads (i.e. strain stiffening). This is seen in all materials regardless of the magnetoelastic nature of the material. To analyze this effect of axial loading, a pre-stressed eigenfrequency simulation was performed for the sensors. In these simulations, the single sensor showed an estimated sensitivity of 2700 ppm/mstrain, while the differential sensor showed 1100 ppm/mstrain. These simulated sensitivities are due only to the strain stiffening effect.

Micro-electrodischarge machining (µEDM) is an attractive technique that can be used for serial or batch-mode micromachining any conductive material [47], [48]. This approach has been previously demonstrated for use in machining of Metglas 2826MB [11]. In this effort, μEDM was used not only to fabricate the sensors, but also the biasing magnets that are described below. The fabricated sensors, single and differential, are shown in Fig. 5.

B. Biasing Magnetic Field and Interrogation Coils

To read out the sensor response, a system consisting of transmit and receive coils was employed (Fig. 6). The transmit coils were used to sweep a range of frequencies within which resonance was expected. The resonant frequency of the sensor was detected by an elevated response in the receive coil. In order to excite a longitudinal mode of vibration, the field lines generated by the transmit coil should loop through the sensor longitudinally. In order to minimize signal feedthrough, the receive coils must be positioned at a null point in the

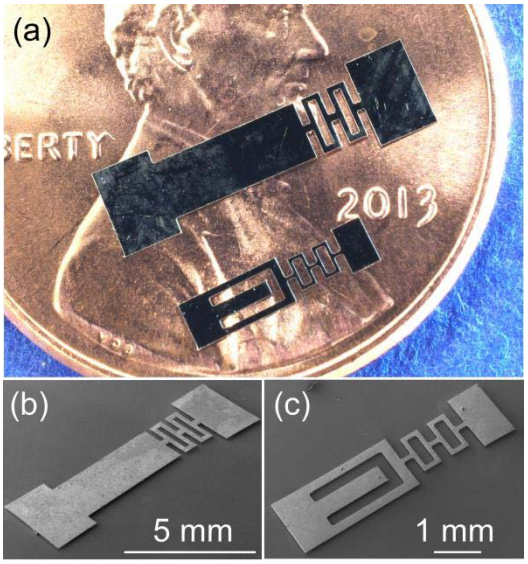

Fig. 5. (a) Microfabricated devices; (b) Single sensor; (c) Differential sensor.

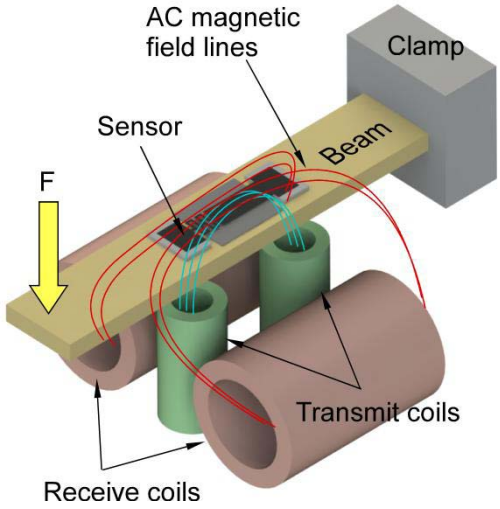

Fig. 6. Coil configuration and test setup used for sensor readout. Blue lines indicate field due to the transmit coils and red lines indicate the field as generated by the sensor and picked up by the receive coils.

transmitted field. The transmit coils were 7 mm in diameter, 20 mm long, and had 10 turns each. The receive coils were 45 mm in diameter, 10 mm long and had 5 turns each. For this work, the sensor was held at a distance of less than 5 mm from the transmit coils. An Agilent model 4395A network analyzer (Agilent Technologies, Santa Clara, CA) was used to read the voltage induced on the receive coil by the sensor response.

To determine the strength of biasing field necessary for device operation, the resonant frequency of the sensors was first experimentally determined using Helmholtz coils to provide the magnetic field. It was found that a biasing field of 5–10 Oe is sufficient for single sensor operation. The differential sensor, being smaller than the single sensor, required a stronger biasing field for operation [49]. For the differential sensor, a bias field of 15–20 Oe was necessary.

C. Sensor Attachment

The single sensor was suspended across two supporting elements (300-μm thick silicon) that offset it from the beam. The longitudinally magnetized Arnokrome 5 bias magnet measuring 6 $\times$ 3 mm^2 was located underneath the suspended sensor. Cyanoacrylate adhesive was used for all attachments. In the case of the differential sensor, to augment the strength of biasing magnetic field, a stack of three longitudinally magnetized Arnokrome 5 magnets was used as the support at each end of the sensor. The magnets each measured 4 $\times$ 2.5 mm^2. As the magnets were in direct contact with the sensor, a larger bias field was provided for sensor operation. Based on magnetometer readings (Model 5180, F. W. Bell, Milwaukie, OR), the magnets provided an estimated 5–10 Oe field required for single sensor and 15–20 Oe field required for the differential sensor. The sensor assemblies for the single and differential sensors are shown in Fig. 1.

IV. Experimental Methods and Results

For testing, the sensors and the biasing magnets were attached to the upper surface of brass cantilevers. The free ends of the cantilevers were pushed down using a force gage (Fig. 6). To calibrate the force used with the strain generated on the beam surface, a commercial strain gage (SGD-5/350-LY13, one-axis general purpose strain gage, Omega Engineering, Inc., Stamford, CT) was first used on the cantilever setup. The reported data is the strain on the beam surface.

The temperature dependence tests were conducted by heating the sensor assembly on a hot plate. Temperature measurements were taken using a thermocouple (Type K, model 5SRTC, Omega Engineering, Inc., Stamford, CT) affixed to the brass beams near the sensors.

A. Single Sensor

The typical single sensor showed an unstrained resonance at 230.8 kHz at 23°C [Fig. 7(a)]. Under applied tensile strain of 1.05 mstrain, the resonant frequency increased to 233.8 kHz. The typical resonance amplitude for the unstrained single sensor was 150 μV; under maximum strain the amplitude reduced to about 50 μV. The decrease in signal amplitude was consistent with expectations because the small signal magnetostrictivity, d, reduces at higher strain levels.

The typical change of resonant frequency as a function of strain is shown in Fig. 7(b). The average sensitivity over this range was typically about 13 $\times$ 10^3 ppm/mstrain. The slope at higher strain levels decreases from a maximum value of 5.2 kHz/mstrain to 1.5 kHz/mstrain. This indicates saturation of ΔE effect as shown in Fig. 2(b). The initial decrease in resonant frequency at small strains can be attributed to the ΔE effect: the localized slope of the stress-strain curve (i.e. the incremental stiffness) does not monotonically increase with applied strain at low levels of strain [30]. This is corroborated by experiments done on similar amorphous alloys [42], [50]. Taking into account the decrease in resonant frequency at lower strains, the single sensors typically showed a dynamic range of 0.05–1.05 mstrain.

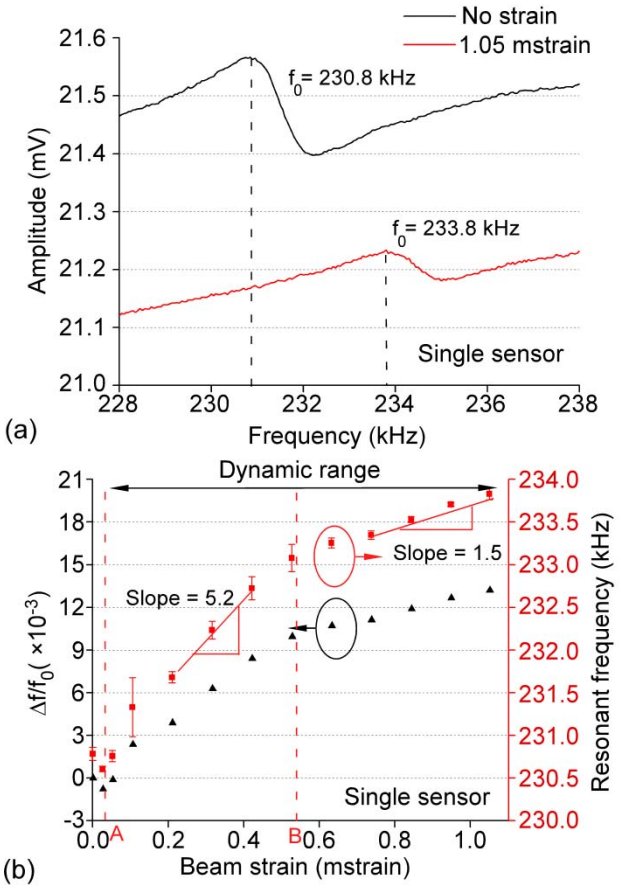

Fig. 7. (a) Resonance of the single sensor at 23°C under no strain and 1.05 mstrain. (b) Resonant frequency and fractional change in resonant frequency as a function of beam strain for a single sensor at 23°C.

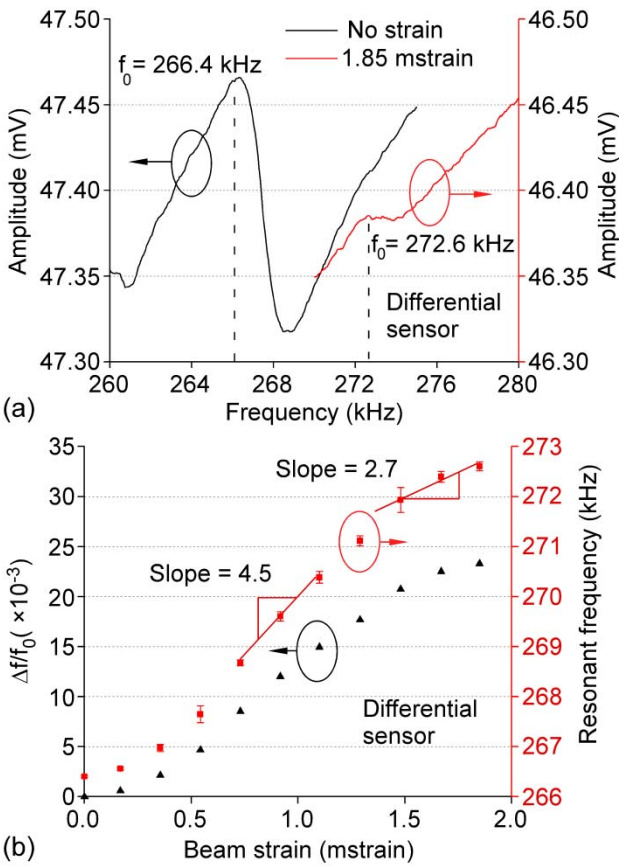

Fig. 8. (a) Resonance of the sensing element of the differential sensor under no strain and 1.85 mstrain at 23°C. (b) Resonant frequency and fractional change in resonant frequency as a function of beam strain for the sensing element of the differential sensor at 23°C.

B. Differential Sensor

For the differential sensor, a typical unstrained resonance for the sensing element was at about 266.4 kHz at 23°C [Fig. 8(a)]. Under applied tensile strain of 1.85 mstrain, the resonant frequency increased to 272.5 kHz resulting in a sensitivity of 12.5 × 10^3 ppm/mstrain. As expected, the amplitude of resonance for the sensing element reduced with increasing strain: the baseline resonance amplitude was 150 μV, while at maximum applied strain the amplitude was less than 10 μV. The reference resonance was at 492.75 kHz. It was experimentally verified that this frequency did not change with applied strains.

The dependence of resonant frequency on applied strain for the sensing element is shown in Fig. 8(b). Unlike the single sensor, the differential sensor did not show a reduction in resonant frequency at strains below 0.05 mstrain. This was because the sensor was biased by a stronger magnetic field at an operating point above the initial dip in stiffness. As was the case with the single sensor, the differential sensor showed a reduced sensitivity at higher strain levels: it fell from a maximum slope of 4.5 kHz/mstrain to 2.7 kHz/mstrain. These measurements were taken at 23°C.

Over the range of temperatures approximately from 20°C to 60°C, the resonant frequency of the reference cantilever varied by −262 ppm/°C [Fig. 9(a)], and that of the sensing element varied by −222 ppm/°C uncorrected by the output of the reference element [Fig. 9(b)]. Based on this and equation (4), the true strain observed in the sensor is plotted in the right axis of Fig. 9(b). If the temperature compensation provided by the cantilever is applied to the simple sensor, its temperature coefficient of resonant frequency changes from −160 ppm/°C uncorrected to 102 ppm/°C corrected [Fig. 9(c)].

V. Discussion

In case of the single sensor, there is an initial reduction in resonant frequency at strain values below 0.05 mstrain. The dynamic range can be extended to lower values by increasing the biasing magnetic field, shifting the baseline resonant frequency to a point in the response plot that is above this dip. It can be seen in Fig. 7(b) shows how initial magnetization or strain can affect the ΔE behavior of magnetoelastic materials and be applied to the strain sensor. A magnetic bias or applied pre-strain can move the baseline operating point to A, where the sensor will show continuous increase with applied strain. Using an even stronger field or higher pre-strain can move the baseline operating point to point B, where the sensor can detect both tensile and compressive strains. It can be seen in Fig. 8 how the experiments for the differential sensor demonstrate this – the magnetic field bias provides an operating point where there is no decrease in resonant frequency with increasing strains.

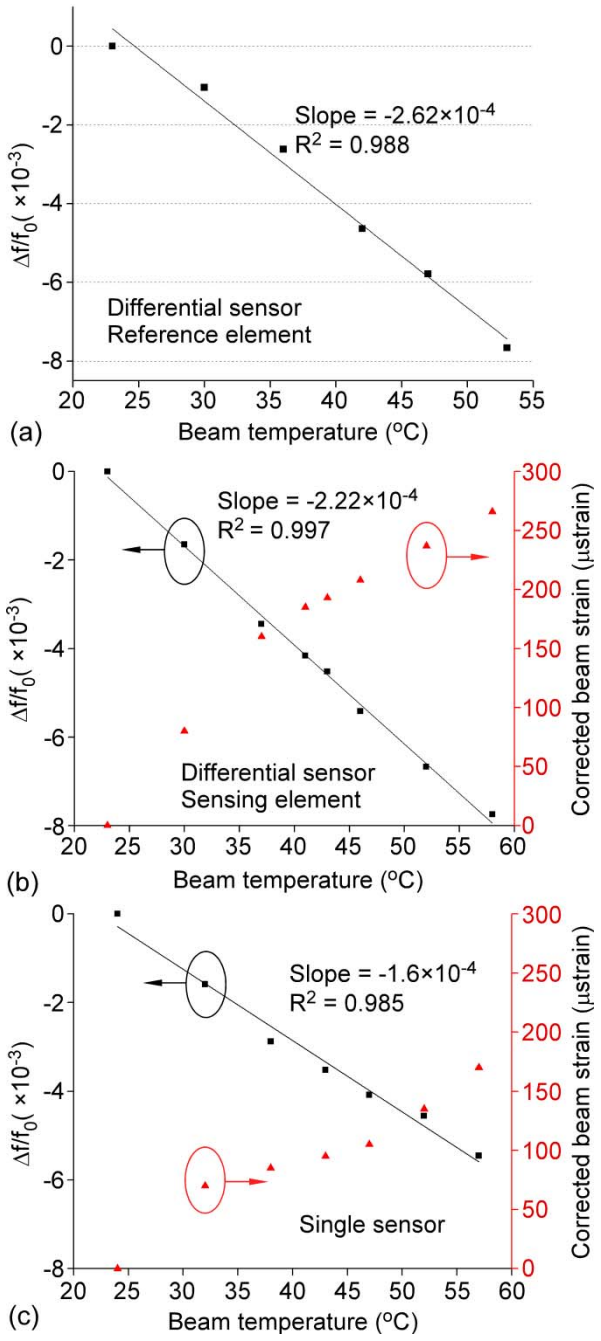

Fig. 9. Temperature compensation as used in differential and single sensor. (a) Fractional change in resonant frequency of the reference resonator as a function of the temperature of the brass beam. (b) Fractional change in resonant frequency of sensing element of the differential sensor and corrected beam strain as a function of temperature. (c) Fractional change in resonant frequency of the single sensor and corrected beam strain as a function of temperature.

As described in section III *A*, a shift in resonant frequency of the device can occur due to strain stiffening. Finite element analysis shows that for the single and differential sensors described in this work, the non-magnetic contributions are 2700 ppm/mstrain and 1100 ppm/mstrain respectively. These are minor compared to the overall measured sensitivity of 13 $\times$ 10^3 ppm/mstrain for the single sensor and 12.5 $\times$ 10^3 ppm/mstrain for the differential sensor. Hence, it can be concluded that it is indeed the ΔE effect which primarily determines the sensitivity of these devices.

In general, a change in temperature affects the resonant frequency of a cantilever through change in Young's modulus or dimension change due to thermal expansion. For a cantilever resonating in the longitudinal mode, the resonant frequency is given by:

$$f_0 = \frac{1}{4L}\sqrt{\frac{E}{\rho(1-\nu^2)}} \tag{5}$$

where, E is the Young's modulus, ρ is the density, ν is the Poisson's ratio, L is the length of the cantilever. The fractional change in resonant frequency resulting from a temperature change can be expressed as:

$$S_\varepsilon(T)\,\Delta T = \frac{\frac{1}{4L(1+\alpha_{TE}\Delta T)}\sqrt{\frac{E(1+\alpha_\gamma \Delta T)(1+\alpha_{TE}\Delta T)^3}{\rho(1-\nu^2)}} - \frac{1}{4L}\sqrt{\frac{E}{\rho(1-\nu^2)}}}{\frac{1}{4L}\sqrt{\frac{E}{\rho(1-\nu^2)}}} \tag{6}$$

ΔT is the temperature change, α_{TE} is the thermal expansion coefficient of Metglas 2826MB and α_γ is the fractional change, with temperature, in the Young's modulus of Metglas 2826MB. However, α_{TE} is 12 ppm/°C – negligible compared to measured $\Delta f/f_0$ – and can thus be ignored for the temperature range under consideration. Equation (6) then simplifies to:

$$S_\varepsilon(T) \approx \frac{1}{\Delta T}\left(\sqrt{(1+\alpha_\gamma \Delta T)} - 1\right) \approx \frac{\alpha_\gamma}{2}. \tag{7}$$

From experimental results, $S_\varepsilon(T)$ for the reference element in the differential sensor is -262 ppm/°C which implies that α_γ is -524 ppm/°C.

The Young's modulus of 2826MB reduces with increasing temperature, lowering the resonant frequency. In contrast, the expansion mismatch of brass and 2826MB, which have thermal expansion coefficients of 19 ppm/°C and 12 ppm/°C, respectively, results in tensile strain, assuming that the strain sensor and the brass beam are at similar temperatures. Hence, these factors influence the resonant frequency of the sensors in opposing manner. For the single sensor, there is a decrease of 1.27 kHz in the resonant frequency for a 35°C increase in temperature. The substantial decrease in resonant frequency with increasing temperature indicates that the decrease in Young's modulus of 2826MB is the dominant parameter influencing the resonant frequency. Considering that the full range of frequencies for the single sensor, observed over the range of applied strain, is about 3 kHz, it is necessary for the temperature variation to be factored into the measurement. For the differential sensor, the sensor resonant frequency falls by 1.85 kHz for a 35°C increase in temperature. Temperature compensation using the response of the reference resonator enables the calculation of the tensile strain caused by the temperature change. In these experiments, the differential sensor and single sensor showed a strain dependence on temperature of 7.45 μstrain/°C (ppm/°C) and 4.52 μstrain/°C (ppm/°C), respectively. This corresponds well with the theoretical expansion mismatch between brass and 2826MB of 7 ppm/°C.

The device operation relies on the magnetic circuit formed by the transmit and receive coils with the sensor. If the sensor rests on a ferromagnetic substrate, it can potentially influence this magnetic circuit. However, the permeability of Metglas 2826MB is much higher than most ferromagnetic materials and the effect of the substrate on sensor read-out will be accommodated by an appropriate calibration on a similar substrate. Another possible concern, especially in relation to possible application in structural health monitoring, is drift and long-term stability. Although the mechanical integrity of the sensor is not a concern, Metglas 2826MB is prone to corrosion in high humidity environments. A thin layer of Parylene-C can be deposited to prevent corrosion if necessary – a method that has been employed in our previous work [38].

The signal quality of the sensor output may be improved in the long term by employing strategies to exploit higher harmonics of the resonant response, thereby reducing feedthrough of the interrogating signal. Pulsed interrogation methods may also reduce signal feedthrough. In addition, the interrogation range can be increased by using larger coils and higher input power for the transmit coils.

VI. Conclusion

This work presents the design, fabrication and experimental results of passive, wireless magnetoelastic strain sensors. Using the ΔE effect of magnetoelastic materials, the devices detect strain as a change in its resonant frequency. The single sensor incorporates only a sensing element, whereas the differential sensor incorporates both a sensing element and a reference resonator. Both sensors use spring structures to attenuate the strain in the sensing element. This architecture allows the sensitivity and dynamic range to be customized. The sensors can be used to measure both tensile and compressive strains by mechanical pre-stressing or by selecting an appropriate magnetic bias field. In the differential sensor, the output of the reference resonator can be used to compensate for resonant frequency change due to the temperature dependence of the Young's modulus of Metglas 2826MB. These sensors are expected to find utility in biomedical and infrastructure monitoring applications.

Acknowledgment

The authors acknowledge Metglas Inc. and ArnoldMagnetic Technologies Corp. for the samples provided for this project.

References

[1] E. H. Leder, D. D'Lima, P. Westerhoff, J. A. Szivek, R. A. Wachs, and G. Bergmann, "Implantable sensor technology: From research to clinical practice," *J. Amer. Acad. Orthopaedic Surgeons*, vol. 20, no. 6, pp. 383–392, 2012.

[2] Y. Hew, S. Deshmukh, and H. Huang, "A wireless strain sensor consumes less than 10 mW," *Smart Mater. Struct.*, vol. 20, no. 10, p. 105032, Oct. 2011.

[3] Y. Jia, K. Sun, F. J. Agosto, and M. T. Quiñones, "Design and characterization of a passive wireless strain sensor," *Meas. Sci. Technol.*, vol. 17, no. 11, pp. 2869–2876, Nov. 2006.

[4] S.-D. Jang, B.-W. Kang, and J. Kim, "Frequency selective surface based passive wireless sensor for structural health monitoring," *Smart Mater. Struct.*, vol. 22, no. 2, p. 025002, Feb. 2013.

[5] K. J. Loh, J. P. Lynch, and N. A. Kotov, "Passive wireless strain and pH sensing using carbo nanotube-gold nanocomposite thin films," *Proc. SPIE*, vol. 6529, p. 652919, Apr. 2007.

[6] J. Chuang, D. J. Thomson, and G. E. Bridges, "Embeddable wireless strain sensor based on resonant RF cavities," *Rev. Sci. Instrum.*, vol. 76, no. 9, pp. 094703-1–094703-7, 2005.

[7] S. Deshmukh and H. Huang, "Wireless interrogation of passive antenna sensors," *Meas. Sci. Technol.*, vol. 21, no. 3, p. 035201, Mar. 2010.

[8] R. Konno, M. Mitsui, and H. Kuwano, "A highly sensitive strain sensor using surface acoustic wave and its evaluation for wireless battery-less sensor network," in *Proc. IEEE Sensors*, Oct. 2007, pp. 796–799.

[9] J. D. Zook, D. W. Burns, J. N. Schoess, and H. Guckel, "Optically resonant microbeams," *Proc. SPIE*, vol. 2383, pp. 6–16, May 1995.

[10] S. R. Green and Y. B. Gianchandani, "Wireless magnetoelastic monitoring of biliary stents," *J. Microelectromech. Syst.*, vol. 18, no. 1, pp. 64–78, 2009.

[11] A. Viswanath, S. R. Green, J. Kosel, and Y. B. Gianchandani, "Metglas–Elgiloy bi-layer, stent cell resonators for wireless monitoring of viscosity and mass loading," *J. Micromech. Microeng.*, vol. 23, no. 2, p. 025010, Feb. 2013.

[12] S. Traxler, J. Kosel, H. Pfützner, E. Kaniusas, L. Mehnen, and I. Giouroudi, "Contactless flow detection with magnetostrictive bilayers," *Sens. Actuators A, Phys.*, vol. 142, no. 2, pp. 491–495, Apr. 2008.

[13] W. J. Karl, A. L. Powell, R. Watts, M. R. J. Gibbs, and C. R. Whitehouse, "A micromachined magnetostrictive pressure sensor using magneto-optical interrogation," *Sens. Actuators A, Phys.*, vol. 81, nos. 1–3, pp. 137–141, Apr. 2000.

[14] F. Seco, J. M. Martín, A. R. Jiménez, and L. Calderón, "A high accuracy magnetostrictive linear position sensor," *Sens. Actuators A, Phys.*, vols. 123–124, pp. 216–223, Sep. 2005.

[15] J. M. Barandiaran, J. Gutierrez, and C. Gómez-Polo, "New sensors based on the magnetoelastic resonance of metallic glasses," *Sens. Actuators A, Phys.*, vol. 81, pp. 154–157, Apr. 2000.

[16] M. L. Johnson *et al.*, "A wireless biosensor using microfabricated phage-interfaced magnetoelastic particles," *Sens. Actuators A, Phys.*, vol. 144, no. 1, pp. 38–47, May 2008.

[17] D. Kouzoudis and C. A. Grimes, "Remote query fluid-flow velocity measurement using magnetoelastic thick-film sensors (invited)," *J. Appl. Phys.*, vol. 87, no. 9, pp. 6301–6303, 2000.

[18] C. A. Grimes, S. C. Roy, S. Rani, and Q. Cai, "Theory, instrumentation and applications of magnetoelastic resonance sensors: A review," *Sensors*, vol. 11, no. 3, pp. 2809–2844, Jan. 2011.

[19] W. J. Fleming, "Magnetostrictive torque sensor performance-nonlinear analysis," *IEEE Trans. Veh. Technol.*, vol. 38, no. 3, pp. 159–167, Aug. 1989.

[20] A. Ben Amor, T. Budde, and H. H. Gatzen, "A magnetoelastic microtransformer-based microstrain gauge," *Sens. Actuators A, Phys.*, vol. 129, nos. 1–2, pp. 41–44, May 2006.

[21] R. Germano, G. Ausanio, V. Iannotti, L. Lanotte, and C. Luponio, "Direct magnetostriction and magnetoelastic wave amplitude to measure a linear displacement," *Sens. Actuators A, Phys.*, vol. 81, nos. 1–3, pp. 134–136, Apr. 2000.

[22] H. T. Savage and C. Adler, "Effects of magnetostriction in amorphous ferromagnets," *Mater. Sci. Eng.*, vol. 99, pp. 13–18, Mar. 1988.

[23] E. L. Tan, A. J. DeRouin, and K. G. Ong, "Magnetoelastic-harmonic stress sensors with tunable sensitivity," *IEEE Sensors J.*, vol. 12, no. 6, pp. 1878–1883, Jun. 2012.

[24] A. Hernando, E. Pina, E. Burgos, C. Prados, and J. M. Gonza, "Magnetoelastic sensor as a probe for muscular activity An in vivo experiment," *Sens. Actuators A, Phys.*, vol. 91, pp. 99–102, Jun. 2001.

[25] H. Oduncu and T. Meydan, "A novel method of monitoring biomechanical movements using the magnetoelastic effect," *J. Magn. Magn. Mater.*, vol. 160, pp. 233–236, Jul. 1996.

[26] T. Huber, B. Bergmair, C. Vogler, F. Bruckner, G. Hrkac, and D. Suess, "Magnetoelastic resonance sensor for remote strain measurements," *Appl. Phys. Lett.*, vol. 101, no. 4, pp. 042402-1–042402-3, 2012.

[27] V. Pepakayala, S. R. Green, and Y. B. Gianchandani, "A passive, wireless strain sensor using a microfabricated magnetoelastic beam element," in *Proc. IEEE Sensors Conf.*, Baltimore, MD, USA, Nov. 2013, pp. 1–4.

[28] H. W. Katz, "Electrostrictive and magnetostrictive systems," in *Solid State Magnetic and Dielectric Devices*. Hoboken, NJ, USA: Wiley, 1959.

[29] J. Gutiérrez, A. Lasheras, J. M. Barandiarán, J. L. Vilas, and M. S. Sebastián, "Improving the magnetoelectric response of laminates containing high temperature piezopolymers," *IEEE Trans. Magn.*, vol. 49, no. 1, pp. 42–45, Jan. 2013.

[30] B. D. Cullity and C. D. Graham, *Introduction to Magnetic Materials*. Hoboken, NJ, USA: Wiley, 2009, p. 257.
[31] R. M. Bozorth, *Ferromagnetism*. Piscataway, NJ, USA: IEEE Press, 1993, p. 684.
[32] G. Engdahl, *Handbook of Giant Magnetostrictive Materials*. New York, NY, USA: Academic, 2000.
[33] R. M. Silva *et al.*, "Magnetic field sensor with Terfenol-D thin-film coated FBG," in *Proc. 22nd Int. Conf. Opt. Fiber Sensors*, vol. 8421. Oct. 2012, p. 84213C.
[34] O. Klaus and Z. Bernhard, "A novel magneto-elastic force sensor design based on Terfenol-D," in *Proc. SENSOR+TEST Conf.*, 2009, pp. 77–82.
[35] C. A. Grimes, Q. Cai, K. G. Ong, and K. Loiselle, "Environmental monitoring using magnetoelastic sensors (Invited Paper)," *Proc. SPIE*, vol. 4097, no. 123, pp. 123–133, 2000.
[36] P. R. Downey and A. B. Flatau, "Magnetoelastic bending of Galfenol for sensor applications," *J. Appl. Phys.*, vol. 97, no. 10, p. 10R505, 2005.
[37] J. H. Goldi, M. J. Gervera, J. Oleksy, G. P. Carmanb, and T. A. Duenasb, "Composite Terfenol-D sonar transducers," *Proc. SPIE*, vol. 3675, pp. 223–234, Mar. 1999.
[38] S. R. Green and Y. B. Gianchandani, "Tailored magnetoelastic sensor geometry for advanced functionality in wireless biliary stent monitoring systems," *J. Micromech. Microeng.*, vol. 20, no. 7, p. 075040, Jul. 2010.
[39] D. Raskin and C. H. Smith, "Applications of amorphous metals: Progress and prospects," in *Amorphous Metallic Alloys*, F. E. Luborsky, Ed. London, U.K.: Butterworths, 1983, p. 397.
[40] M. Brouha and J. van der Borst, "The effect of annealing conditions on the magneto-mechanical properties of Fe-B-Si amorphous ribbons," *J. Appl. Phys.*, vol. 50, no. B11, pp. 7594–7596, 1979.
[41] P. M. Anderson, "Magnetomechanical coupling, $\triangle$E effect, and permeability in FeSiB and FeNiMoB alloys," *J. Appl. Phys.*, vol. 53, no. 11, pp. 8101–8103, 1982.
[42] B. S. Berry and W. C. Pritchet, "Magnetoelastic phenomena in amorphous alloys," *AIP Conf. Proc.*, vol. 292, no. 1, pp. 292–297, 1976.
[43] Metglas Inc. (2013, Oct. 18). *Magnetic Alloy 2826MB (Nickel-Based) Technical Bulletin* [Online]. Available: http://www.metglas.com
[44] Arnold Magn. Technol. Corp. (2013 Oct. 18). *Rolled Products Strip & Foil Catalogs & Literature* [Online]. Available: http://www.arnoldmagnetics.com/Thin_Gauge_Strip_and_Foil_Literature.aspx
[45] G. Hausch and E. Török, "Elastic, magnetoelastic, and thermal properties of some ferromagnetic metallic glasses," *Phys. Status Solidi*, vol. 50, no. 1, pp. 159–164, Nov. 1978.
[46] M. K. Jain, Q. Cai, and C. A. Grimes, "A wireless micro-sensor for simultaneous measurement of pH, temperature, and pressure," *Smart Mater. Struct.*, vol. 10, no. 2, pp. 347–353, Apr. 2001.
[47] T. Masaki, K. Kawata, and T. Masuzawa, "Micro electro-discharge machining and its applications," in *Proc. IEEE Int. Workshop Micro Electro Mech. Syst.*, Feb. 1990, pp. 21–26.
[48] K. Takahata and Y. B. Gianchandani, "Batch mode micro-electro-discharge machining," *J. Microelectromech. Syst.*, vol. 11, no. 2, pp. 102–110, Apr. 2002.
[49] D.-X. Chen, E. Pardo, and A. Sanchez, "Demagnetizing factors for rectangular prisms," *IEEE Trans. Magn.*, vol. 41, no. 6, pp. 2077–2088, Jun. 2005.
[50] E. Török and G. Hausch, "Magnetoelastic effects of some ferromagnetic metallic glasses," in *Rapidly Quenched Metals III*. London, U.K.: The Metals Society, 1978, pp. 105–108.

Venkatram Pepakayala received a B.Tech. degree in electronics and telecommunication engineering from Nagpur University, Nagpur, India, in 2010, and an M.S. degree in electrical engineering from the University of Michigan, Ann Arbor, USA, in 2012, where he is working toward a Ph.D. degree in electrical engineering.

He is currently a Graduate Student Research Assistant with the Department of Electrical Engineering and Computer Science, University of Michigan. His research interests include magnetoelastic wireless sensors and actuators with focus on applications as implantable microdevices.

Scott R. Green received a B.S. in mechanical engineering from Rose-Hulman Institute of Technology in 2003, and an M.S. (2008) and Ph.D (2009) in mechanical engineering from the University of Michigan, Ann Arbor, with a focus in Microsystems. He worked as a senior design engineer at Stryker Corporation in the Instruments division from 2003-2005. He currently is an Assistant Research Scientist at the University of Michigan, Ann Arbor. Research interests include wireless magnetoelastic sensors and actuators, miniature implantable medical systems, and miniature and microfabricated high-vacuum sputter ion pumps.

Yogesh B. Gianchandani (S'83–M'85–SM'05–F'10) is a Professor at the University of Michigan, Ann Arbor, with a primary appointment in the Electrical Engineering and Computer Science Department and a courtesy appointment in the Mechanical Engineering Department. He also serves as the Director for the Center for Wireless Integrated MicroSensing and Systems (WIMS^2).

Dr. Gianchandani's research interests include all aspects of design, fabrication, and packaging of micromachined sensors and actuators (http://www.eecs.umich.edu/~yogesh/). He has published about 300 papers in journals and conferences, and has about 35 U.S. patents issued or pending. He was a Chief Co-Editor of *Comprehensive Microsystems: Fundamentals, Technology, and Applications*, published in 2008. Dr. Gianchandani has served on the editorial boards and program committees of a number of conferences and journals. From 2007 to 2009, he also served at the National Science Foundation as the program director for Micro and Nano Systems within the Electrical, Communication, and Cyber Systems Division (ECCS).